Boundary-Layer Meteorology (2005) 117: 259–273
DOI 10.1007/s10546-004-1427-2

WAVE FLOW SIMULATIONS OVER ARCTIC LEADS

THORSTEN MAURITSEN[1,*], GUNILLA SVENSSON[1] and BRANKO GRISOGONO[2]

[1]*Department of Meteorology, Stockholm University, S-10691 Stockholm, Sweden;* [2]*Department of Geophysics, Faculty of Science, Zagreb, Croatia*

(Received in final form 29 June 2004)

Abstract. We investigate the flow over Arctic leads using a mesoscale numerical model, typical of both summer and winter, under idealised conditions. We find that Arctic leads may be the source of standing atmospheric internal gravity waves during both seasons. The summertime wave may be compared with the wave generated by a small ridge, though with the phase reversed. The mechanism for exciting the wave is found to be the internal boundary layer developing due to horizontal variations in surface temperature and roughness length. During the more exploratory wintertime simulations, with substantial temperature difference between the lead and the ice surface, we find that secondary circulations and intermittent wave-breaking may occur. The effects of the lead appear far downstream.

Keywords: Arctic, Gravity waves, Ice leads, Intermittent and elevated turbulence, Wave-breaking.

1. Introduction

The Arctic ocean is covered with ice throughout the year, with the average ice thickness varying with season around a few metres. However, due to the divergence of the upper ocean currents and the stress excerted on the ice surface by winds, both ridges with thicker ice and cracks with open water or thin ice, called leads, appear throughout the year (Lindsay and Rothrock, 1995; Miles and Barry, 1998). The leads introduce surface heteorogeneities that affect the overlying atmosphere, and are believed to be important sources of heat, moisture, chemical species and aerosols for the Arctic atmospheric boundary layer. A high resolution satellite image for cloud free conditions is shown in Figure 1 (NASA Visible Earth site: http://visible-earth.nasa.gov/). The leads are revealed to be long and narrow, with a typical width of a few kilometres or less.

The ice-surface temperature may vary substantially throughout the year, as can be seen from Figure 2 (Persson et al., 2002), though during the Arctic summer, the ice-surface temperature is usually close to the melting point. For the Surface Heat Budget of the Arctic Ocean Project (SHEBA, Uttal et al., 2002) site this occurs from the end of May to the beginning of September.

*E-mail: thorsten@misu.su.se

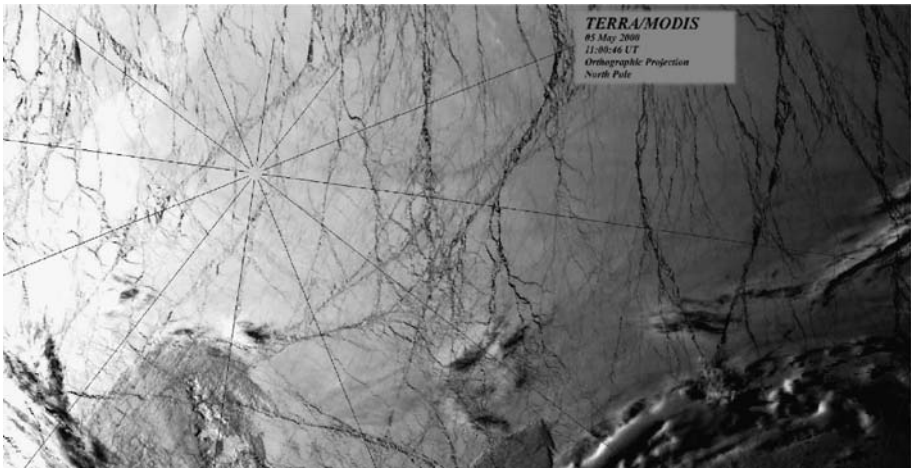

Figure 1. In this satellite image, the sea-ice appears in shades of grey and areas of open water, or recently refrozen sea surface, appear black. Note a considerable number of leads appearing as dark networks of lines. The irregular shapes in the lower part of the image are clouds. The image was acquired by the Moderate resolution Imaging Spectroradiometer (MODIS), on May 5, 2000. The image resolution is 1 km.

Shorter events of slightly lower surface temperatures occur throughout this period, and are usually associated with cloud free conditions and large net radiative loss of surface heat. During wintertime the ice surface temperature can be below −40 °C.

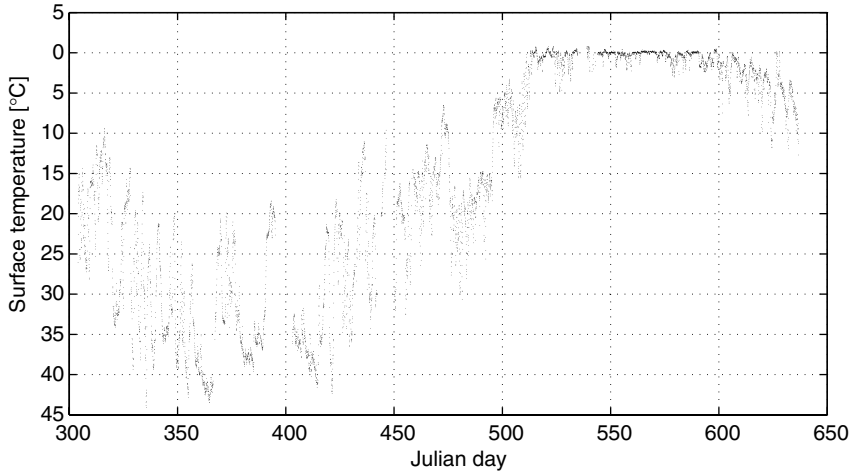

Figure 2. Best estimate of the surface temperature based on three different radiometers measured at the Surface Heat Budget for the Arctic ocean (SHEBA) site. Julian day 1 corresponds to January 1, 1997, and accordingly Julian day 366 is January 1, 1998.

Large-eddy simulations have been used to investigate the problem of estimating the heat flux from leads under idealised conditions. For instance, Zulauf and Krueger (2003) used a wide range of lead widths, different cross-wind speeds and winter-like conditions, to estimate both the heat flux and plume penetration height. The numerical experiments were performed with a temperature difference between the ice surface and the open lead of 27 K.

It is well-known that orographic obstacles can be a source of atmospheric gravity waves (Queney, 1948; Smith, 1979). These can have a wide range of effects such as wave drag, clear air turbulence and hydraulic jumps among others (e.g. Grisogono, 1995). Moreover, gravity waves can transport momentum and energy far away from their sources (e.g. Nappo, 2002). It was also pointed out by Malkus and Stern (1953) that a flat island, which is warmer than the surrounding sea, can be a source of internal gravity waves. It is, however, not so well-known that surface heteorogeneities of temperature and roughness can be sources of atmospheric gravity waves, even in the absence of orography.

Paluch et al. (1997) analysed aircraft data from the Beaufort Arctic Storms Experiment (BASE) flying over both open sea and ice-covered sea during autumn. They found that short gravity waves, with horizontal wavelengths of approximately 1.1–2.8 km, and convective roll vortices were present in an area with many open leads. The temperature difference between the open leads and the ice surface was 5–10 K. Furthermore, enhanced vertical motions were observed downwind of a lead using remote sensing sodars during the Arctic Leads Experiment (LEADEX), see Ruffieux (1995), and interpreted as gravity waves interacting with the thin boundary layer.

Bigg et al. (1996) reported observations of rapid changes in the Arctic atmospheric aerosol and several gas concentrations that occured during the Arctic Ocean Expedition 1991 (Leck et al., l996). Bigg (1997) suggested that part of the observed variability was caused by intermittent turbulent bursts from breaking gravity waves at the top of the boundary layer. Since large gradients of temperature, moisture and chemical species often exist across the boundary-layer inversion, mixing events from the free troposphere to the boundary layer may cause rapid variations in the concentration of chemical species.

It is the goal of this study to show that Arctic leads can be a source of standing gravity waves. Subsequently we provide an insight into the complexities that may arise when these waves interact with the stable boundary layer.

2. Model

The numerical model used in the present study is the Coupled Ocean/-Atmosphere Mesoscale Prediction System (COAMPS^{TM}), version 2.0

(Hodur, 1997)[1]. It was developed at the Naval Research Laboratory Monterey, California and is run operationally at the Fleet Numerical Meteorology and Oceanography Center.

Only the atmospheric component of the model was used in this study; it solves the non-hydrostatic, compressible dynamical equations as in Klemp and Wilhelmson (1978). Sound waves are resolved explicitly, but are filtered away. The prognostic variables are three dimensional winds, potential temperature, pressure perturbation, water vapour, cloud droplets, raindrops, ice crystals, snowflakes and turbulent kinetic energy (TKE). The model grid is of the Arakawa-C staggered type; the grid is also staggered in the vertical and is terrain following. Fourth-order advection was used in the present study.

The model uses a second-order turbulence closure model described by Yamada (1977) with modified constants found in Mellor and Yamada (1982). It handles TKE as a prognostic variable, while the remaining second-order moments are calculated diagnostically from the mean state variables and TKE. This is formally called a level-2.5 closure. The length scale used in the boundary layer was a modified version of Blackadar (1962),

$$l = \lambda_0 \left(\frac{kz}{kz + \lambda_0} \right),$$

where k is the von Karman constant and λ_0 is the asymptotic boundary layer scale, defined by:

$$\lambda_0 = \alpha \frac{\int_0^\infty \sqrt{\mathrm{TKE}} z \, dz}{\int_0^\infty \sqrt{\mathrm{TKE}} \, dz},$$

where α is a tuning constant set to 0.1 in stable stratification, while it gradually increases to 0.3 in unstable conditions. The Blackadar length scale has a limit kz at the ground and λ_0 for large z.

2.1. SET-UP

The model domain was chosen to be two dimensional with periodic lateral boundary conditions; in the horizontal direction 600 gridpoints were used with a resolution of 500 m. Such high horizontal resolution can be applied because the model is non-hydrostatic. Since the model resolves sound waves, a time step of one second was needed to inhibit sound-wave phase speeds of up to 360 m s^{-1}. In the vertical, a total of 99 levels were used, with levels at 2, 6, 10, 16, 24 m etc., used in and near the boundary layer, with a transition to a constant vertical resolution of 150 m in the free troposphere. The model top was at 13 km.

[1] The COAMPS™ homepage, http://www.nrlmry.navy.mil/projects/coamps/, supplies additional information

Horizontal numerical diffusion was applied using a fourth-order filter in order to damp poorly resolved small-scale features. The form of the filter is $k\nabla^2(\nabla^2\beta)$, where β is the prognostic variable in question. The size of the diffusion coefficient, K, was chosen to be as small as possible in each case, in order to avoid excessive damping of divergent atmospheric gravity waves. A sponge layer was placed in the upper 30 model levels, from 8.5 km upwards, in order to accomodate at least two vertical wavelengths of the dominant gravity wave. Also here the strength of the sponge layer was considered in each case, in order to minimise reflections and optimise the damping.

The roughness length for the ice surface was set to 10^{-2} m and for the ocean surface to about 5×10^{-5} m. The sensitivity to the roughness length was tested, but found to be insignificant for the major conclusions of the present study. Moist and radiative processes along with Coriolis effects were neglected, even though we believe that these processes are often important for the Arctic boundary layer.

An ice lead was located in the middle of the two-dimensional model domain, and the ice surface kept at constant temperature. The sea surface temperature was chosen to be at the freezing point of salt water. A total of 7 gridpoints in the middle of the domain were defined to be sea surface. The edges were smoothed linearly in order to reduce small-scale numerical noise from the transition from ice to sea surface. The effective width of the lead is therefore about 3 km. The initial atmospheric stratification was chosen to be constant throughout with a buoyancy frequency of $N = 0.02\ \mathrm{s}^{-1}$.

3. Results

Here we will present the results of three selected simulations. The experiments are listed in Table I. The temperature difference, the background horizontal wind and the section where the experiment is described are also listed.

3.1. Summer case

The results of the summer simulation are shown in Figure 3a–c. Here a stably stratified boundary layer is formed upstream of the lead, and an elevated

TABLE I
Summary of simulations

Description	ΔT(K)	U(m s^{-1})	Section
Summer lead case	3	5.0	3.1
Winter lead case, weak winds	27	2.5	3.2
Winter lead case, moderate winds	27	5.0	3.2

inversion between 120 and 160 m capping a turbulent layer of decreased stratification appears.

A convective internal boundary layer extending up to approximately 80 m forms above the open lead, see Figure 3a, resulting in vertical mixing of heat and momentum. The convective mixing increases the average wind speed in the boundary layer above the lead, and due to continuity there has to be

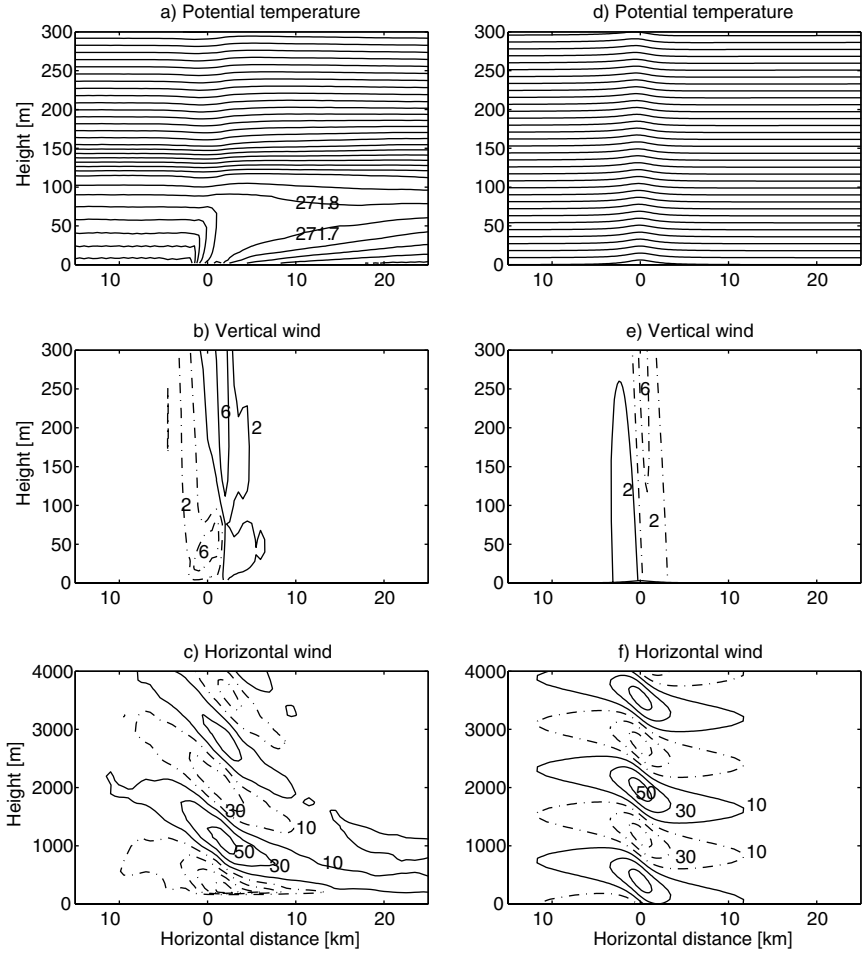

Figure 3. Comparison of the summertime lead simulation, (a–c), and an analytical solution for flow over a small ridge, (d–f). Upper panels show the boundary-layer potential temperatures with a contour interval of 0.1 K. Middle panels show the vertical wind. Solid and dotted curves represent positive and negative anomalies, respectively. The contour interval is 0.004 m s^{-1}. Lower panels show the free tropospheric horizontal wind deviation from mean with a contour interval of 0.02 m s^{-1}. The lead is placed at $x = 0$ and the wind is from left to right. No zero lines are shown. The simulation time is 9 h. Only a small part of the model domain is shown. Note also the different vertical scales in (c) and (f) with respect to the upper four panels.

downward vertical motion above the lead, see Figure 3b. Downstream, a stable internal boundary layer develops against the residual layer. This results in a decreased average wind speed in the boundary layer, and a small positive vertical velocity.

A weak standing wave appears in the free troposphere, see Figure 3c; it is generated by the boundary-layer pattern already described in Figure 3a and b. The horizontal wind component of the wave has an amplitude of 0.05–0.10 m s^{-1} and when compared with the background wind of 5 m s^{-1} indicates that linear wave theory is applicable. The horizontal wavelength is seen to be approximately 12 km, which is about four times the effective width of the lead and the ridge. For constant background wind and stratification the Taylor–Goldstein equation for standing gravity waves reads (e.g. Nappo, 2002):

$$\frac{d^2\hat{w}}{dz^2} + \left[\frac{N^2}{U^2} - k^2\right]\hat{w} = 0, \tag{1}$$

where $\hat{w}$ is the vertical wind amplitude, U is the background wind speed and k is the horizontal wavenumber. The term in the brackets can be considered as the square of a vertical wavenumber, m. Using the horizontal wavelength to give $k = 2\pi/L_x$ gives a vertical wavelength $L_z = 2\pi/m$ of 1580 m. This is close to the 1.6 km as found in the simulations (Figure 3c).

From the linear wave flow over a surface corrugation, a set of relations can be found connecting the amplitude of the wind and potential temperature perturbations, w', u' and θ' from the background state to the vertical and horizontal wavenumbers, background wind and corrugation amplitude, H (e.g. Nappo, 2002):

$$w' = -UHk, \tag{2}$$

$$u' = -UHm, \tag{3}$$

$$\theta' = H\frac{\partial\theta}{\partial z}. \tag{4}$$

The open lead may be thought of as equivalent to an orographic ridge. For scaling purposes, it may be sufficient to replace the surface corrugation wavelength with a typical width of the ridge and the corrugation amplitude with the ridge height (Nappo, 2002). Using these relations, we can estimate the equivalent height of the ridge needed to generate the wave that the summer lead creates. Choosing for instance $u' \approx 0.06$ m s^{-1} (Figure 3c) gives an equivalent height of 3 m from (3).

We can compare the results of the simulation with an analytical solution of flow over a ridge of the bell-shaped type:

$$h(x) = \frac{Hb^2}{x^2 + b^2},$$

where $h(x)$ is the orography height, H is the maximum ridge height and b is the half-width of the ridge. A solution has been found by Queney (1948) for the linearised two-dimensional, hydrostatic, non-rotating, steady state flow equations using the Buossinesq approximation. This is a good approximation so long as the free flow Froude number, $F_r = U/NH$, is much larger than unity. The results are shown in Figure 3d to f for $b = 2$ km and $H = 3$ m. The standing gravity wave found in the free troposphere is quite similar to the wave in the summer lead case.

Using Equations (2)–(4) to estimate the equivalent height is supported by observations of gravity waves by Paluch et al. (1997). In an autumn case, with several narrow open or recently re-frozen leads, gravity waves were found (their Figure 5). Taking $L_x \approx 1.4$ km, $U \approx 8$ m s^{-1} and $w' \approx 0.3$ m s^{-1}, gives an equivalent height of 8 m. This is higher than in our simulated case, which is likely due to the larger temperature difference between the ice surface and the leads in the observed autumn case.

The waves in the case of the summer lead simulations and the analytical solution for the ridge differ on a few points. Most pronounced is the 180 degree phaseshift of the wave, see Figure 3c and f. This is because the mechanisms for generating the wave are basically different. In the orographic wave case, the air is displaced upward by the ridge, leading to the positive low-level vertical wind on the upwind side and the negative vertical wind on the downwind side of the ridge simply due to continuity and the pressure distribution, see Figure 3e. In the lead case on the contrary, the convective internal boundary layer produces more effective downward transport of momentum increasing the horizontal wind locally in the boundary layer. This leads to the downward wind on the upwind side and the upward wind on the downwind side seen in Figure 3b. Therefore, the wave is phase-shifted 180 degrees compared to the orographic wave case.

Another, less pronounced, difference is found in the downstream region. For the lead case a secondary wave appears. In Figure 3c it hardly appears, because it was weaker than the primary wave found above the lead. The wave was found to be excited by the stably stratified internal boundary layer developing downstream of the lead in a similar way as the primary wave. The horizontal wavelength of the secondary wave is longer than for the primary wave, due to the longer characteristic scale of the stably stratified internal boundary layer.

It is important to remember that internal gravity waves can only exist in stably stratified atmospheres. The long-lived stable boundary layer, which is common in the Arctic, is in direct contact with the stratified free troposphere. Here $N^2/U^2 > k^2$ from the surface upwards, for realistic lead sizes. Equation (1) then allows for oscillating solutions, yielding internal gravity waves. On the contrary, the mid-latitude nocturnal boundary layer is capped by the residuallayer created by the daytime convective boundary layer (e.g. Stull,

1988). There $N \approx 0$, which allows only for damped, evanescent solutions of (1).

3.2. WINTER CASE

Having established that summertime Arctic leads can be a source of relatively weak linear gravity waves, we move on to consider a wintertime case with a substantial temperature difference between the lead and the ice surface. The atmospheric conditions were chosen to be close to those used in Zulauf and Krueger (2003), with a temperature difference of 27 K. This is well within the range of observed wintertime surface temperatures of Persson et al. (2002) shown in Figure 2. Two cases, one with $U = 2.5$ m s^{-1} and one with $U = 5$ m s^{-1} were inspected. We used the same model set-up as for the summertime case, with the only difference being that the numerical horizontal diffusion was increased slightly.

The results of the two simulations are shown in Figure 4. A back ground stable boundary layer exists upstream of the lead. In both cases convection rapidly heats the air above the lead, penetrating the background boundary-layer inversion up to 250–350 m as a consequence of the large temperature difference. For large-eddy simulations, with the same background conditions, Zulauf and Krueger (2003) found a penetration height of 270 m, which is practically the same as found with the mesoscale model. Further, a 10-m wind speed increase from 1.2 to 3.2 m s^{-1} and a cross-lead increase in air temperature of 4 K is similar to the results of Zulauf and Krueger (2003), see their Figure 9. Note how the 10-m wind speed exceeds the background wind of 2.5 m s^{-1} for both models. The sensible heat flux at the first model level was on average 580 W m^{-2}, while Zulauf and Krueger (2003) only found approximately 300 W m^{-2}. There can be several reasons for this discrepancy. For instance, Pinto et al. (2003) showed that the surface roughness is important for the heat flux. Also, the surface-layer parameterisations in the two models may be different and sensitive to vertical resolution, since the lowest level is not at the same height.

In Figure 5 we inspect vertical profiles of potential temperature, wind and TKE for the weak and moderate wind cases 25 km downstream of the lead. In the weak wind case, the convection dominates over the background wind. A secondary circulation with a near surface counterflow opposite to the background wind in the downstream region is formed. The counterflow supplies the lead region with cold surface air, generating a sharp inversion below 50 m, as seen in Figure 5a and b. In contrast, in the moderate wind case, the background wind dominates over the convection. Here a stably stratified internal boundary layer develops downstream of the lead, since no counterflow is established.

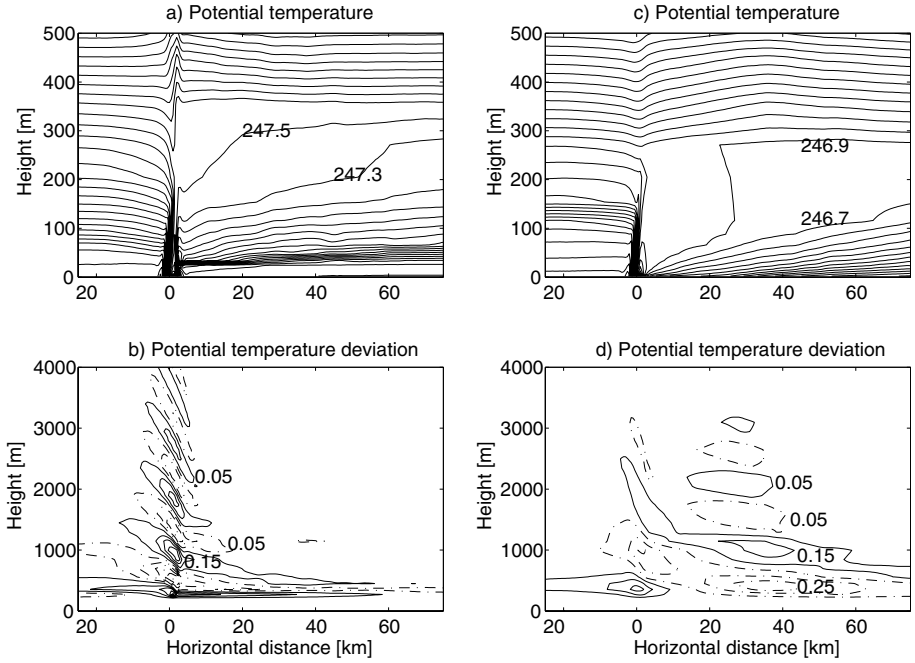

Figure 4. Results of two wintertime simulations with 27 K temperature difference between the lead and the ice surface after 12 h of integration. In one case, (a and b), U = 2.5 m s^{-1} whereas in the other case, (c and d), U = 5 m s^{-1}. In (a) and (c) the boundary-layer potential temperature is shown with a contour interval of 0.2 K, and in (b) and (d) the free troposphere potential temperature deviation from the mean is shown with a contour interval of 0.1 K. Dash dotted are negative values. Note also the variable vertical scales.

The difference in the boundary-layer structure results in a distinct difference in the wave pattern found in the free troposphere, see Figure 4b and d. In both cases the primary wave appears above the lead, although only the moderate wind case exhibits a secondary wave. This is probably because of the lack of a developing stably stratified internal boundary layer in the weak wind case. The secondary wave extends approximately 50 km downstream of the lead, and appears to have a horizontal wavelength on the order of 100 km, which is nearly two orders of magnitude more than the width of the lead itself. We find a vertical wavelength $L_z = 0.8$ km in Figure 4b and twice that in 4d, which is expected from Equation (1). The wave amplitudes are more than an order of magnitude stronger than in the summer case. The effect of the increased horizontal numerical diffusion, (mentioned in Section 2.1) in the winter case simulations can be seen from Figures 4b and d. The wave amplitude decreases with height away from the source, as it is damped by the horizontal diffusion.

The presence of the lead affects the vertical structure of TKE far downstream of the lead. Figures 5c and f show a two-layer structure of the

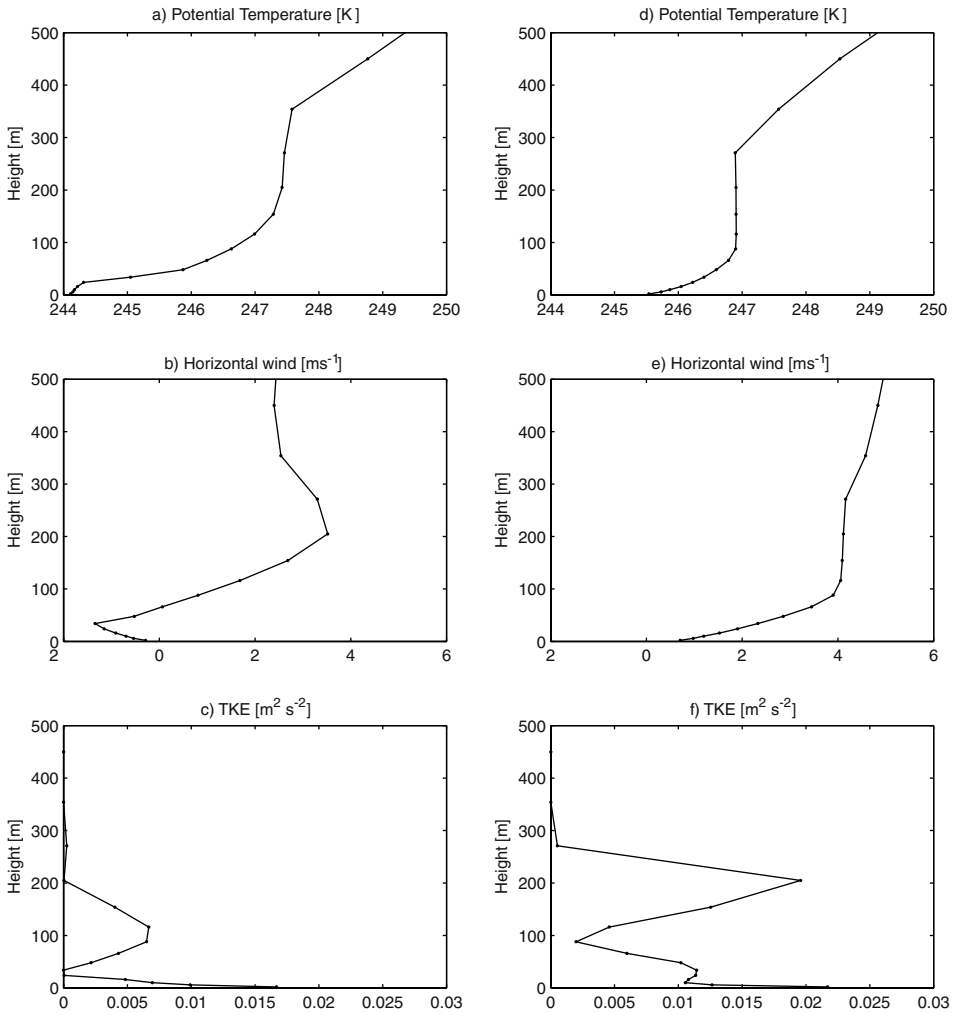

Figure 5. Vertical profiles of the potential temperature, the horizontal wind and the TKE 25 km downstream of the lead, for the cases presented in Figure 4. Here (a–c) is for the $U = 2.5$ m s^{-1} case while (d–f) is for the $U = 5$ m s^{-1} case. The dots indicate where the model levels are located.

TKE 25 km from the lead. Close to the surface shear-driven turbulence is found in both simulations. In the weak wind case a local maximum of TKE is found at 100 m, which is found to be due to the shear between the two opposite directed jets seen in Figure 5b. For the moderate wind case a stronger elevated maximum is found at 200 m. This, on the other hand, is due to a convective instability of the flow seen in the potential temperature profile (Figure 5c).

The moderate wind case has elevated convective downstream turbulence, which is due to wave-induced cooling at the top of the boundary layer seen in

Figure 4d. This is related to wave-breaking due to convective instabilities described for instance in Nappo (2002). We inspect the temporal evolution of TKE downstream of the lead in Figure 6. After a few hours the two-layer structure of TKE appears, which remains for the entire simulation. While the lower shear driven layer reaches steady state after about 7 h, the upper convective layer is found to be intermittent throughout the simulation. This behaviour somewhat resembles the quasi-propagating hydraulic jump found in Enger and Grisogono (1998), see their Figures 4 and 5, though it cannot be directly compared since their results apply to a gravity wave generated by a ridge. Note that the high levels of TKE during the first hour of the simulation is partly artificial, because the horizontal winds are prescribed constant throughout at the beginning of the simulation, creating infinite shear at the surface during the model spin-up.

4. Conclusions

A numerical mesoscale model is employed to investigate lower tropospheric flow over Arctic leads. We have shown that Arctic leads can be a source of standing atmospheric gravity waves. In the first case we considered conditions representative of the summertime Arctic. The temperature difference

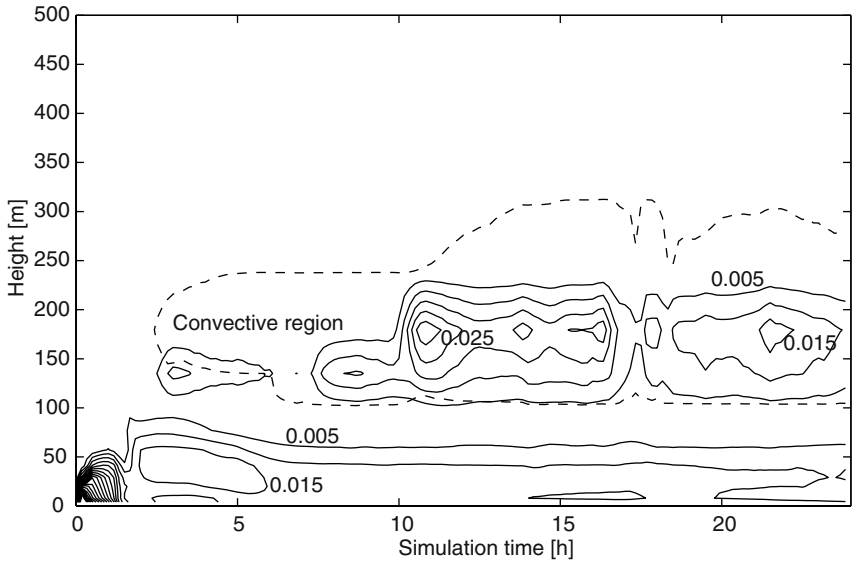

Figure 6. Time evolution of TKE in the boundary layer 25 km downstream of the lead for the 5 m s^{-1} background wind case. The solid contour lines are TKE for every 5×10^{-3} m^2 s^{-2}. The dashed line indicates convective instability, as inferred from the potential temperature profile.

between the ice and lead surface was set to 3 K and the atmosphere was stably stratified throughout. A standing linear gravity wave appeared above the lead, and the wave flow over the lead was found to be similar to the flow over a small ridge. The results are supported by observational evidence from the literature.

Above the lead a convective internal boundary layer penetrates the background stable boundary layer. The strong convective turbulence increases the downward momentum flux, which accelerates the air horizontally above the lead. This in turn generates downward vertical motion due to continuity. On the downwind side of the lead a stable internal boundary layer develops more gradually against the residual of the lead convection. This decelerates the air, giving an upward component to the wind. Because the background atmosphere is stably stratified from the surface upwards, the perturbation is allowed to propagate away from the lead as a gravity wave. It is important to note that this is only possible for the long-lived stable boundary layer. The mid-latitude nocturnal boundary layer is usually capped by a near-neutral residual layer, which prevents internal gravity wave propagation.

In two exploratory simulations with conditions typical of the wintertime Arctic, the wave may interact with the stable boundary layer. In a weak wind case the convection dominated over the background wind generating a secondary circulation, which reversed the downstream surface winds. The resulting vertical shear caused an elevated layer of turbulence. In the second, moderate wind case wave-breaking caused convective instabilities in an elevated layer up to 50 km downstream of the lead. The wave-breaking turbulence was found to be intermittent.

The Arctic region is stably stratified during long periods. Observations of surface fluxes in stable and very stably stratified boundary layers show that surface fluxes are not well described by existing theories that assume local surface-generated continuous turbulence (Poulos and Burns, 2003). In this study, we have identified leads as sources of gravity waves. However, the magnitude of the wave from a single summertime lead is small and comparable to a wave excited from a low hill (few metres high): the sea-ice contains ridges of similar heights. These ridges are, unlike the leads, not wide enough to excite intense internal gravity waves. Although small, considering the number of leads in the Arctic, these waves may still potentially interact with each other, increase in amplitude during cold seasons, break and contribute to surface turbulence. This would be a non-local intermittent source of near-surface turbulence.

Acknowledgements

We thank our colleagues in the SHEBA Atmospheric Surface Flux Group, Ed Andreas, Chris Fairall, Peter Guest, and Ola Persson for collecting and

processing the data used in Figure 2. We acknowledge the Naval Research Laboratory for making the COAMPS^{TM} model available. The MODIS satellite image was supplied by NASA through their freely available website, Visible Earth: http://visibleearth.nasa.gov/. Support for this work was from the Swedish Research Council contract 621-2001-1846.

References

Bigg, E. K., Leck, C., and Nilsson, E. D.: 1996, 'Sudden Changes in Arctic Atmospheric Aerosol Concentrations During Summer and Autumn', *Tellus* **48B**(2), 254–271.

Bigg, E. K.: 1997, 'A Mechanism for the Formation of New Particles in the Atmosphere', *Atmos. Res.* **43**(2), 129–137.

Blackadar, A. K.: 1962, 'The Vertical Distribution of Wind and Turbulent Exchange in Neutral Atmosphere', *J. Geophys. Res.* **67**, 3095–3102.

Enger, L. and Grisogono, B.: 1998, 'The Response of Bora-type Flow to Sea Surface Temperature', *Quart. J. Roy. Meteorol. Soc.* **124**(548), 1227–1244.

Grisogono, B.: 1995, 'Wave Drag Effects in a Mesoscale Model with Higher-order Closure Turbulence Scheme', *J.Appl. Meteorol.* **34**(4), 941–954.

Hodur, R. M.: 1997, 'The Naval Research Laboratory's Coupled Ocean/Atmosphere Mesoscale Prediction System (COAMPS^{TM})', *Mon. Wea. Rev.* **125**(7), 1414–1430.

Klemp, J. B. and Wilhelmson, R. B.: 1978, 'Simulation of Three-dimensional Convective Storm Dynamics', *J. Atmos. Sci.* **35**(6), 1070–1110.

Lindsay, R. W. and Rothrock, D. A.: 1995, 'Arctic Sea Ice Leads from Advanced very High Resolution Radiometer Images', *J. Geophys. Res.* **100**(C3), 4533–4544.

Malkus, J. S. and Stern, M. E.: 1953, 'The Flow of a Stable Atmosphere Over a Heated Island, part I', *J. Meteorol.* **10**, 30–41.

Mellor, G. L. and Yamada, T.: 1982, 'Development of a Turbulence Closure Model for Geophysical Fluid Problems', *Rev. Geophys. Space Phys.* **20**(4), 851–875.

Miles, M. W. and Barry, R. G.: 1998, 'A 5-year Satellite Climatology of Winter Sea Ice Leads in the Western Arctic', *J. Geophys. Res.* **103**(C10), 21723–21734.

Nappo, C. J.: 2002, *An Introduction to Atmospheric Gravity Waves*, International geophysics series, Vol. 85, Academic Press, 276 pp.

Paluch, I. R., Lenschow, D. H. and Wang, Q.: 1997, 'Arctic Boundary Layer in the Fall Season Over Open and Frozen Sea', *J. Geophys. Res.* **102**(D22), 25955–25971.

Persson, P. O. G., Fairall, C. W., Andreas, E. L., Guest, P. S., and Perovich, D. K.: 2002, 'Measurements Near the Atmospheric Surface Flux Group Tower at SHEBA: Near-surface Conditions and Surface Energy Budget', *J. Geophys. Res.* **107**(Cl0).

Pinto, J. O., Alam, A., Maslanik, J. A. Curry, J. A., and Stone, R. S.: 2003, 'Surface Characteristics and Atmospheric Footprint of Springtime Arctic leads at SHEBA', *J. Geophys. Res.* **108**(C4).

Poulos, G. S. and Burns, S. P.: 2003, 'An Evaluation of Bulk Ri-Based Surface Layer Flux Formulas for Stable and Very Stable Conditions with Intermittent Turbulence', *J. Atmos. Sci.* **60**(20), 2523–2537.

Queney, P.: 1948, 'The Problem of Air Flow Over Mountains: A Summary of Theoretical Studies', *Bull. Amen. Meteorol. Soc.* **29**, 16–26.

Ruffieux, D., Persson, P. O. G., Fairall, C. W., and Wolfe, D. E.: 1995, 'Ice Pack and Lead Surface Energy Budgets During LEADEX 1992', *J. Geophys. Res.* **100**(C3), 4593–4612.

Smith, R. B.: 1979, 'Influence of Mountains on the Atmosphere', *Adv. Geophys.* **21**, 87–217.

Stull, R. B.: 1988, *An Introduction to Boundary Layer Meteorology*, Kluwer Academic Publishers, Dordrecht, 666 pp.

Uttal, T., Curry, J. A., McPhee, M. G., Perovich, D. K., Moritz, R. E., Maslanik, J. A., Guest, P. S., Stern, H. L., Moore, J. A., Turenne, R., Heiberg, A., Serreze, M. C., Wylie, D. P., Persson, P. O. G., et al.: 2002, 'Surface Heat Budget of the Arctic Ocean', *Bull. Amer. Meteorol. Soc.* **83**(2), 255–275.

Yamada, T.: 1977, 'Numerical Experiment on Pollutant Dispersion in a Horizontally Homogeneous Atmospheric Boundary Layer', *Atmos. Environ.* **11**(11), 1015–1024.

Zulauf, M. A. and Krueger, S. K.: 2003, 'Two-dimensional Numerical Simulations of Arctic Leads: Plume Penetration Height', *J. Geophys. Res.* **108**(C2).